AIAA SciTech Forum
January 3-7, 2022, San Diego, CA & Virtual
AIAA SCITECH 2022 Forum

10.2514/6.2022-0593

Check for updates

Optical Characterization of Flowfield behind Pin Array in Supersonic Duct

Philip A. Lax[1], Skye Elliott[2], Stanislav Gordeyev[3], and Sergey B. Leonov[4]
University of Notre Dame, Notre Dame, IN, 46556

This work is focused on an experimental characterization of the flowfield structure, parameters, and dynamics in vicinity of a supersonic mixer composed of a pin array. The instrumentation employed is essentially non-intrusive and includes fast schlieren visualization, a spanwise integrating technique, and acetone Mie scattering, a planar technique. A temperature dependence of the acetone seeding technique enables the recognition of small detailed structures in the mixing layer behind the pins as visualized by planar Mie scattering. An analysis of the data acquired by these complementary methods allows reconstruction of a three-dimensional portrait of supersonic flow interaction with a discrete pin array, including the shock waves structure, forefront separation zone, shock-induced separation zone, shear layer and a mixing zone behind the pins.

Downloaded by Stanislav Gordeyev on December 30, 2021 | http://arc.aiaa.org | DOI: 10.2514/6.2022-0593

1. Introduction

Shock wave/boundary layer interactions (SWBLIs) resulting from circular cylinders imbedded in supersonic turbulent boundary layers have been widely studied, including the associated flow patterns [1], shock structures [2], and pressure distributions [3]. Numerical techniques have been used to study cylinders normal to the wall [4] and parallel to the wall [5] as well as axisymmetric steps [6]. Some scaling laws and correlations [7] have been found, but only for simple geometries. Rather than a single cylinder, the current study is focused on spanwise cylindrical pin array in supersonic turbulent boundary layers. Such pin arrays are candidates for supersonic mixing enhancement as well as hypersonic vehicle inlet/engine control.

Far from a solid boundary, a single cylinder in supersonic crossflow is characterized by a bow shock in front of the cylinder and an unsteady subsonic wake immediately behind the cylinder. Further behind the cylinder the flow is again accelerated to supersonic velocity. The flowfield can be characterized by a complex interaction between shock waves and vortices generated by the cylinder. When multiple cylinders are placed in an array across the flow, the front bow shocks merge. Flow immediately behind the combined bow shocks is subsonic, and a curved sonic line exists between the cylinders past which the flow is again supersonic. The resulting flowfield is schematically illustrated in Fig. 1.

Near the solid boundary, the bow shock in front of a cylinder separates into a forward separation shock and a rear reattachment shock near the base of the cylinder, forming a classic lambda shape. The intersection of these shocks is referred to as the triple point. A separated flow region exists beneath the lambda shock. Just below the triple point a high pressure supersonic jet penetrates the flow separation zone, creating two horseshoe vortices and a supersonic region immediately in front of the cylinder. At the upper end of the

[1] Graduate Student, Department of Aerospace and Mechanical Engineering, AIAA Student Member.
[2] Graduate Student, Department of Aerospace and Mechanical Engineering, AIAA Student Member.
[3] Associate Professor, Department of Aerospace and Mechanical Engineering, AIAA Associate Fellow.
[4] Research Professor, Department of Aerospace and Mechanical Engineering, AIAA Associate Fellow.

Copyright © 2022 by Philip A.
Lax, Skye Elliott, Stanislav Gordeyev, and Sergey B. Leonov. Published by the American Institute of Aeronautics and Astronautics, Inc., with permission.

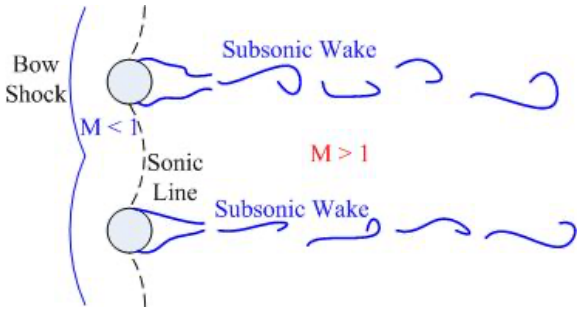

Figure 1. Flow schematics around the pins in the spanwise plane.

Downloaded by Stanislav Gordeyev on December 30, 2021 | http://arc.aiaa.org | DOI: 10.2514/6.2022-0593

cylinder, the bow shock curves around the tip of the cylinder and continues propagating downstream. The nature of the interaction is complex, leading to many features that are largely under-investigated but may be of a great importance for the mixing efficiency.

After conventional flow diagnostics such as a spanwise-integrated schlieren imaging, detailed flow visualization may be performed by seeding the flow with tracer particles. However, obtaining uniform seeding in supersonic flow is challenging due to difficulties in mixing the added tracer particles. Also, the seeded particles must be small enough in order for the particles to faithfully follow the flow without slipping. At the same time, the presence of the particles should not affect the flow structure. These issues can be circumvented by adding a condensable vapor to the high pressure supply of the tunnel. As the static temperature of the gas decreases as it passes through the nozzle, the vapor condenses, forming small (nano/micro-scale), uniformly distributed droplets. These droplets may be visualized by laser scattering. Since the droplets may be smaller or larger than the wavelength of light used, the scattering of light is described by Mie scattering theory, which converges to the Rayleigh scattering approximation in the limit of very small droplets. Since these droplets will reevaporate if the gas temperature is increased, this method is also sensitive to temperature changes in the flow, such as those across shocks.

The objective of this work is a visualization of the flowfield behind an array of cylindrical pins in supersonic crossflow using Schlieren imaging and Mie/Rayleigh scattering of condensed droplets.

2. Experimental Setup and Instrumentation

The SBR-50 at the University of Notre Dame is a supersonic blowdown wind tunnel with interchangeable Mach 2 and Mach 4 nozzles, with the Mach 2 nozzle being used here. The test section has an upstream cross section of 76.2×76.2 mm with a 1-degree expansion on the top and bottom walls and a total length of 610 mm. Quartz side windows and fused silica upper and lower windows provide optical access to the test section. Stagnation conditions of the facility are p_0 = 1-4 bar and T_0 = 300-750 K provided by resistive heaters, with steady-state runtimes of approximately 0.5 s. Working fluids include filtered, dried air as well as pure N_2 and gas mixtures. A total of 48 static pressure ports are distributed along the upper and lower test sections walls, and a 16-probe Pitot rake is installed at the end of the test section. Standard instrumentation of the facility includes a 64-channel pressure scanner (Scanivalve MPS4264) with 800 Hz acquisition rate.

Flow seeding was performed by adding liquid acetone in the gas supply to the high pressure tank of the facility. The liquid acetone injection is atomized in a fine spray, and the gas is passed through an in-line

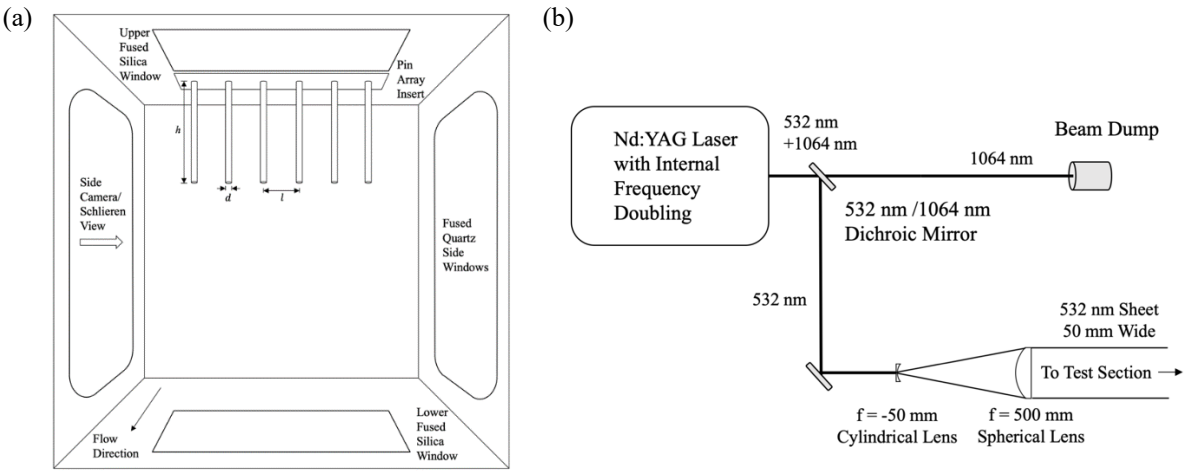

Figure 2. Illustrations of (a) perspective view of test section interior and (b) laser sheet forming arrangement.

mixer with internal baffles to ensure a homogeneous mixture. Since the vapor pressure of acetone is approximately 30 kPa at room temperature, the liquid is easily evaporated. Nitrogen gas from compressed gas cylinders is used as a working fluid to provide an inert carrier gas for the acetone.

2.1. Test geometry

Interchangeable pin array inserts are composed of stainless steel cylindrical pins press fit into threaded aluminum inserts which are installed on the upper wall of the test section. The pin array inserts are composed of 7 pins each, and have a pin diameter d of 2.5 mm, pin spacing l of 10 mm center-to-center, and pin height h of 25 mm, 10 mm, and 5 mm. Rectangular fused silica windows 50 mm in the spanwise direction and 100 mm in the streamwise direction are the flush mounted on both the upper and lower test section walls downstream of the pin array inserts to provide optical access to the wake region. An illustration of the test section interior is provided in Fig. 2(a).

2.2. Schlieren technique

The schlieren light source consists of a high-current broadband white LED (Luminus Devices CFT-90-WCS-X11-VB600) powered by a pulsed LED driver (PicoLAS GmbH LDP-V 240-100 V3.3) with pulse width 20ns-10μs at 40-240 A, 200ns being used in this test series. While the LED is rated for 27A continuous, in pulsed operation it may be used with up to 200A without damage. The light source is focused using a 50mm f=32mm aspheric condenser lens (Thorlabs ACL50832U-A) and a 50mm f=350mm achromatic doublet (Edmund Optics 49-289-INK) and collimated and refocused using two 120mm f/8.3 refractors (Celestron Omni XLT 120). Imaging is performed with a high-speed CMOS camera (Phantom v2512) fitted with a relay lens (Nikon 200mm f/4 AI-s). Two schlieren techniques are utilized: a traditional knife edge method and a central dot method. A knife edge method is sensitive to density gradients in one direction, while a central dot method is sensitive to density gradients in all directions.

Downloaded by Stanislav Gordeyev on December 30, 2021 | http://arc.aiaa.org | DOI: 10.2514/6.2022-0593

Downloaded by Stanislav Gordeyev on December 30, 2021 | http://arc.aiaa.org | DOI: 10.2514/6.2022-0593

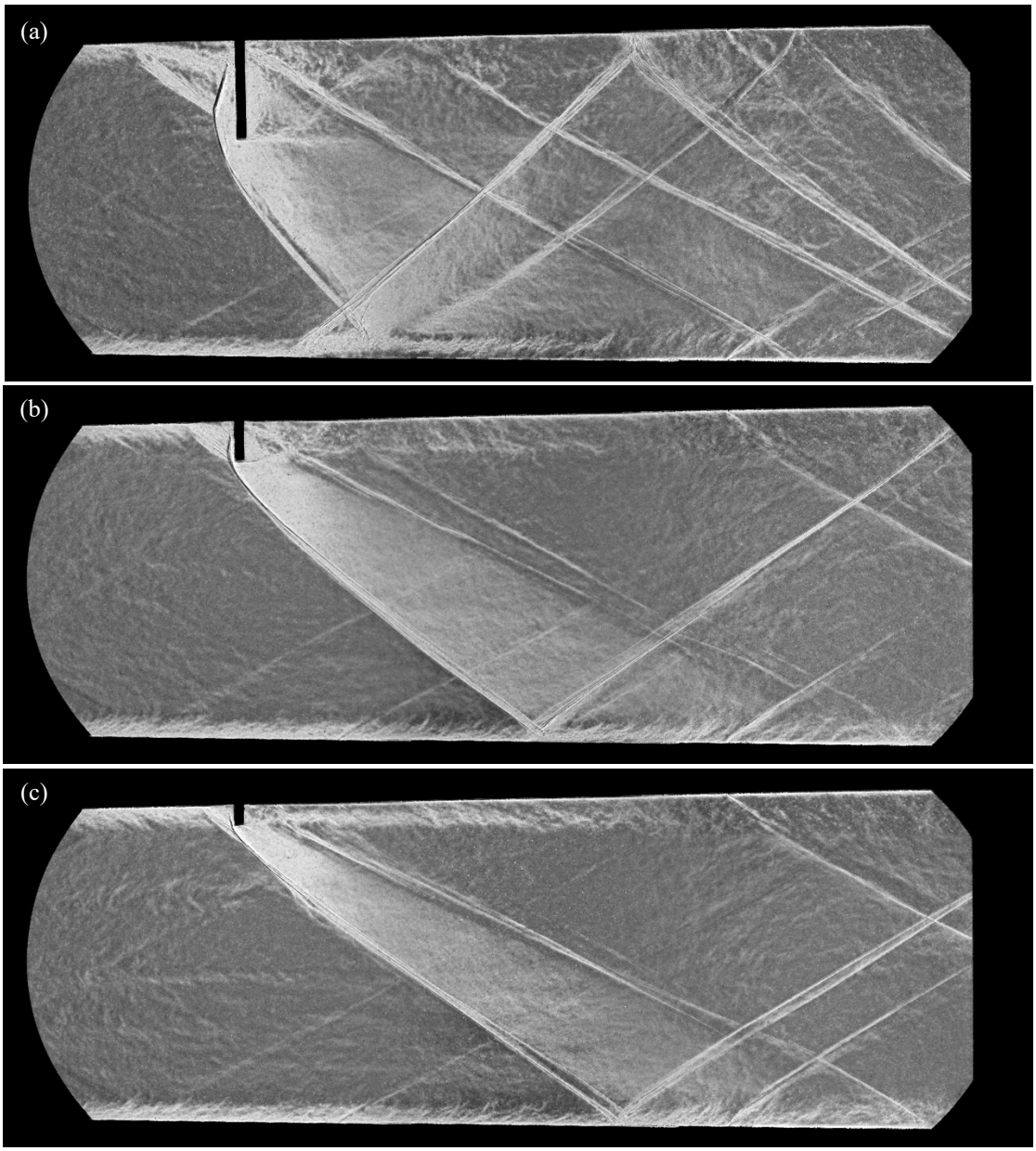

Figure 3. Instantaneous composite central dot schlieren images of (a) 25 mm pins, (b) 10 mm pins, and (c) 5 mm pins. Mach 2 flow is from left to right.

2.3. Mie scattering

Mie scattering is the elastic scattering of light from particles whose diameters may be either smaller or larger than the wavelength of the light. The flow is seeded with acetone at a concentration of approximately 2% by volume. Expansion of flow from room temperature is adequate to condense the acetone vapors, forming acetone microdroplets. Laser sheet forming for Mie scattering uses a 10 Hz nanosecond pulsed Nd:YAG laser frequency doubled to 532nm and the sheet forming optics illustrated in Fig. 2(b).

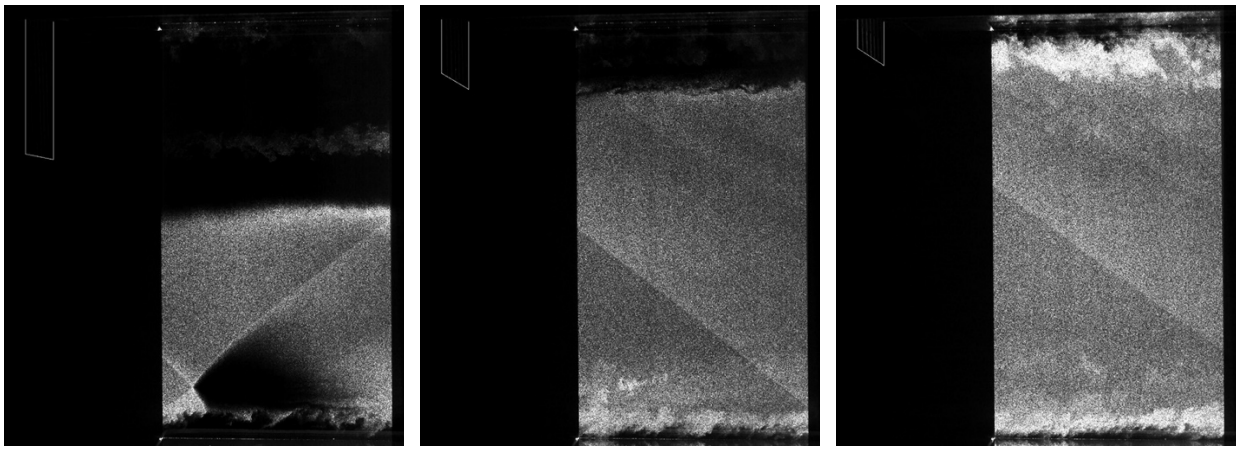

(a) 25 mm pins (b) 10 mm pins (c) 5 mm pins

Figure 4. Mie scattering images taken in flow-wise direction. Pin array location is outlined in white.

Downloaded by Stanislav Gordeyev on December 30, 2021 | http://arc.aiaa.org | DOI: 10.2514/6.2022-0593

3. Observations and Results

3.1. General flow structure and Schlieren imaging

In general, the shock structure near a wall-normal circular cylinder is composed of a forward separation shock which joins a normal bow shock and a reattachment shock closer to the base of the cylinder at the triple point to form the classic lambda shock structure. This structure is visible in the experimental composite schlieren images in Fig. 3, each subfigure consisting of three schlieren images stitched together. A subsonic separation region is formed beneath the lambda shock base, while the bow shock curves around the tip of the cylindrical pin to form a nearly straight oblique shock that reflects off the opposite wall. A second reattachment shock is formed near the downstream base of the pin. A shear layer is formed at the pin tips, which propagates downstream. The schlieren images represent a typical, commonly known picture of an obstacle interaction with supersonic flow. Despite the high resolution of the images, the details of the flowfield in the mixing layer are basically not recognizable by the schlieren method due to low gas density gradients in this area.

3.2. Mie scattering

The Mie scattering images in Fig. 4 were taken using an intensified camera and a 50 mm wide 532nm laser sheet positioned on the centerline of the test section and against the upstream edge of the fused silica window. Stagnation conditions are $P_0 = 2.6$ bar and $T_0 = 300$ K. Similarly to Figure 3, oblique and reflected shocks and a turbulent boundary layer are visible in Fig. 4(a), as well as weak corner shocks in Fig. 4(b) and (c).

Condensed acetone droplets evaporate in regions of high temperature, such as those downstream of strong shock structures. A notable feature in the images of Fig. 4 is the near total lack of scattering downstream of the pin arrays due to the normal or nearly normal shocks positioned in front of them. A region devoid of acetone droplets and thus Mie scattering is also present near the bottom wall of Fig. 4(a) downstream of the reflected oblique shock due to high temperatures in this region. Since the gas temperature in the boundary layer is close to stagnation conditions, Mie scattering is not present in the boundary layer immediately next to a solid wall.

Two exceptions to this trend of droplet evaporation are in the shear layer downstream of the pin tips in Fig. 4(a) and to a certain degree in Fig. 4(b), as well as in some structures in the turbulent shear layer near the walls. Since both the pin tip shear layer and the turbulent boundary layer on the upper wall must pass

Downloaded by Stanislav Gordeyev on December 30, 2021 | http://arc.aiaa.org | DOI: 10.2514/6.2022-0593

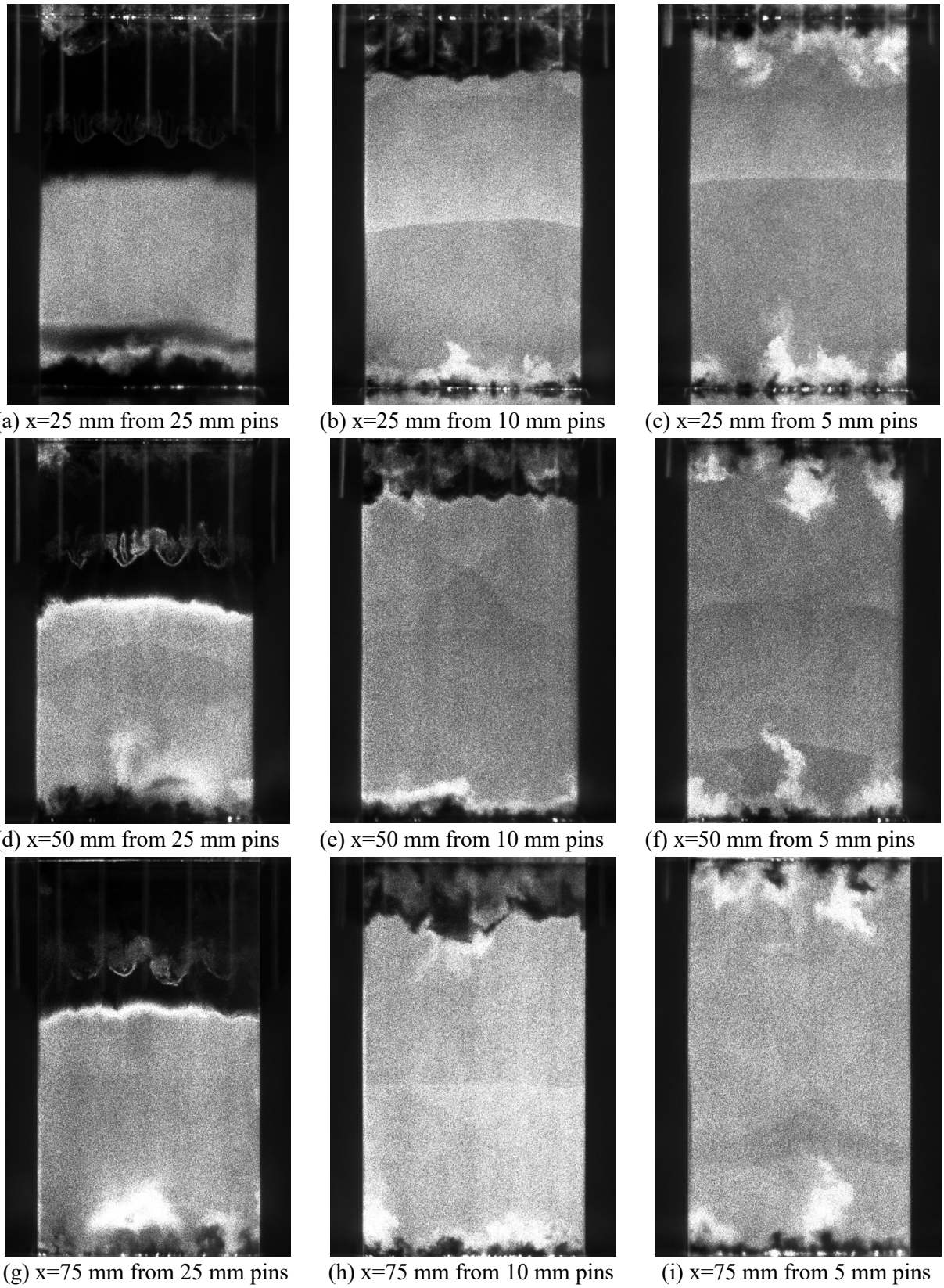

(a) x=25 mm from 25 mm pins (b) x=25 mm from 10 mm pins (c) x=25 mm from 5 mm pins

(d) x=50 mm from 25 mm pins (e) x=50 mm from 10 mm pins (f) x=50 mm from 5 mm pins

(g) x=75 mm from 25 mm pins (h) x=75 mm from 10 mm pins (i) x=75 mm from 5 mm pins

Figure 5. Mie scattering cross-flow images.

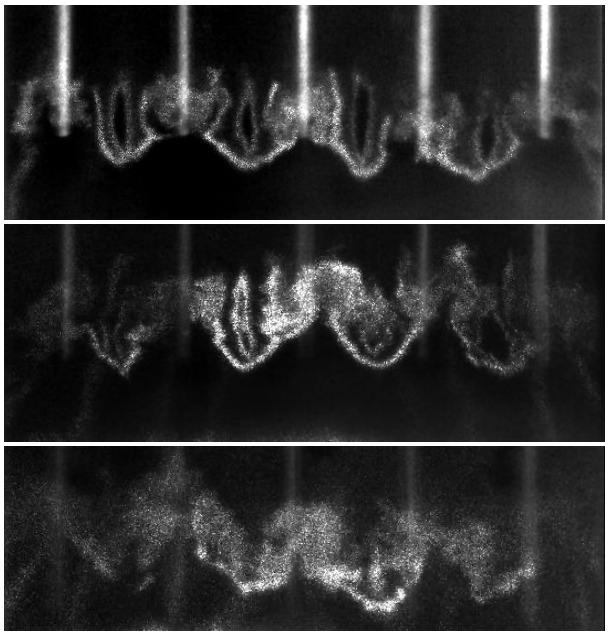

Figure 6. Pin tip structures from 25 mm pins at (a) x=25 mm, (b) x=50mm, and (c) x=75 mm downstream.

through the high-temperature lambda shock region upstream of the pin arrays, some portion of this flow must either experience rapid local expansion and the corresponding re-condensation of acetone droplets or ingest relatively cooler gas from another region in the flow.

3.3. Cross-flow features by Mie scattering

Cross-flow Mie scattering images were taken using the same laser arrangement as streamwise images but with the cylindrical diverging lens rotated 90 degrees. Images were taken through a fused silica window on the vacuum tank on the centerline of the test section using a telephoto lens (Nikon 200mm f/4 and Tokina 400mm f/5.6), and are presented in Figs. 5 and 6. The pins are visible in the images due to light scattering off the stainless steel surfaces.

The oblique shock, seen as a diagonal line in Fig. 4, is visible as a horizontal line in Fig. 5 as it cuts through the plane of the image. The shock is not perfectly two-dimensional, and it curves slightly near the side walls. A turbulent boundary layer is visible on both the upper and lower walls. The droplet-free region behind the pins in Fig. 4 are also visible in Fig. 5. The droplet-free region behind the oblique shock impingement in Fig. 4(a) is visible as a dark strip near the bottom of Fig. 5(a). Large scale structure is visible in interface between the warmer droplet-free region behind the pins and the cooler droplet-filled region, and the size of the structures is similar to the pin-to-pin spacing. These structures grow in size as the flow moves downstream and the two regions mix together.

Also visible in Fig. 5 are fine-scaled structures near the end of the pin tips. These structures are especially evident for the 25 mm pins, which are shown in detail with enhanced contrast in Fig. 6. These structures are currently attributed to the pin-end longitudinal vortices, though the details require further clarification.

3.4. Enhanced scattering regions

Apparent in the Mie scattering images of Figs. 5-7 are regions of enhanced laser scattering, resulting in brighter regions of the flow. These regions are generally near an interface between warmer and cooler gas,

Downloaded by Stanislav Gordeyev on December 30, 2021 | http://arc.aiaa.org | DOI: 10.2514/6.2022-0593

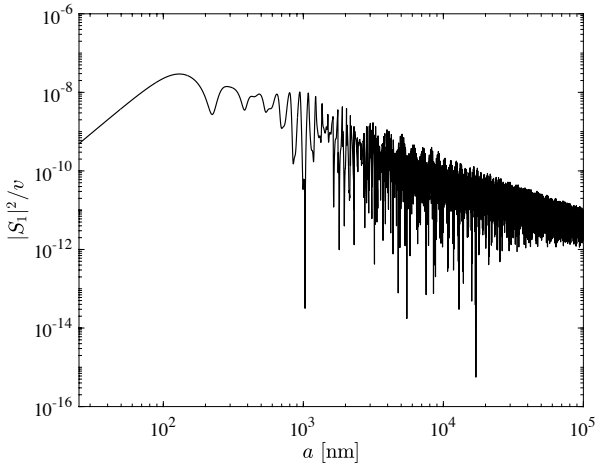

Figure 8. Mie scattering amplitude scaled by droplet volume.

such as the turbulent boundary layer in Fig. 4(c) or at the boundary of the droplet-free region behind the pin tips in Fig. 5(g). Since interfaces between warmer and cooler gas are regions with droplet evaporation and re-condensation, droplets in these regions are smaller and more numerous than in more equilibrated regions of the flow. As shown in Figure 8, the magnitude of the scattering amplitude function S_1 [10] scaled by the droplet volume v has a maximum at a radius of about 130nm. While the scattering of a spherical droplet increases with increasing droplet radius, the scattering intensity per unit volume of droplets has a maximum at a droplet radius of approximately $\lambda/4$. This results in increased light scattering in regions with numerous small droplets.

4. Conclusion

Cylindrical wall-normal pin arrays of various heights have been studied using schlieren imaging and acetone Mie scattering. These methods have been used to visualize flow structures such as the lambda shock region, reattachment shocks, shock wave impingements, and the supersonic shear layer originating from the pin tips.

The detailed visualization of the fine structure of the flowfield in the shear layer demonstrates that the Mie scattering method is a powerful tool for the reconstruction of flowfield details when the gas density gradients are too low to be well-detectable with commonly used techniques such as schlieren, aero-optical distortions detection, or even laser differential interferometry (LDI). In terms of sensitivity, this method is especially beneficial when the flow temperature is accurately adjustable, as is realizable with SBR-50 facility.

Most features of the flowfield acquired with these optical methods are well predictable. However, the description of a few peculiarities requires further analysis. Among them is the structure of the mixing layer behind the pin array where the pin-generated vorticity leads to the generation of complex flow structures in the supersonic zone as visualized by Mie scattering. Another focus of upcoming efforts is a quantitative analysis of fast schlieren video and Shack-Hartmann datasets to reveal details of the flow velocity distribution behind the pin array.

Downloaded by Stanislav Gordeyev on December 30, 2021 | http://arc.aiaa.org | DOI: 10.2514/6.2022-0593

Acknowledgements

This work was partially supported by Institute for Flow Physics and Control (FlowPAC), University of Notre Dame. The authors also would like to thank Dr. Matthew Kemnetz for valuable comments and suggestions about the experiments.

References

[1] Sedney, R., and Kitchens, C. W., "Separation ahead of Protuberances in Supersonic Turbulent Boundary Layers," *AIAA Journal*, Vol. 15, No. 4, 1977, pp. 546-552. URL https://doi.org/10.2514/3.60658.

[2] Leidy, A. N., Neel, I. T., Tichenor, N. R., and Bowersox, R. D. W., "High-Speed Schlieren Imaging of Cylinder-Induced Hypersonic-Shock-Wave–Boundary-Layer Interactions," *AIAA Journal*, Vol. 58, No. 7, 2020, pp. 3090-3099. URL https://doi.org/10.2514/1.J059193.

[3] Gang, D., Yi, S., and Niu, H., "Highly separated axisymmetric step shock-wave/turbulent-boundary-layer interaction," *Journal of Visualization*, No. 24, 2021, pp. 461-470. URL https://doi.org/10.1007/s12650-020-00723-1.

[4] Hahn, P. V., and Frendi, A., "Experimental investigation of supersonic turbulent flow over cylinders with various heights," *AIAA Journal*, Vol. 51, No. 7, 2013, pp. 1657-1666. URL https://doi.org/10.1007/s12650-020-00723-1.

[5] Dudley, J. G., and Ukeiley, L., "Numerical Investigation of a Cylinder Immersed in a Supersonic Boundary Layer," *AIAA Journal*, Vol. 50, No. 2, 2012, pp. 257-270. URL https://doi.org/10.2514/1.J050647.

[6] Chandola, G., Huang, X., and Estruch-Samper, D., "Highly separated axisymmetric step shock-wave/turbulent-boundary-layer interaction," *J. Fluid Mech.*, Vol. 828, pp. 236-270. URL https://doi.org/10.1017/jfm.2017.522.

[7] Dolling, D. S., and Bogdonoff, S. M., "Scaling of Interactions of Cylinders with Supersonic Turbulent Boundary Layers," *AIAA Journal*, No. 19, No. 5, 1981, pp. 655-658. URL https://doi.org/10.2514/3.7805.

Downloaded by Stanislav Gordeyev on December 30, 2021 | http://arc.aiaa.org | DOI: 10.2514/6.2022-0593